THE JOURNAL OF BIOLOGICAL CHEMISTRY VOL. 292, NO. 7, pp. 2611–2623, February 17, 2017

Phosphorylation at Ser^8 as an Intrinsic Regulatory Switch to Regulate the Morphologies and Structures of Alzheimer's 40-residue β-Amyloid (Aβ40) Fibrils*

Received for publication, September 7, 2016, and in revised form, December 5, 2016 Published, JBC Papers in Press, December 28, 2016, DOI 10.1074/jbc.M116.757179

Zhi-Wen Hu[‡], Meng-Rong Ma[‡], Yong-Xiang Chen[‡], Yu-Fen Zhao[‡], Wei Qiang[§1], and Yan-Mei Li[‡¶2]

From the [‡]Key Laboratory of Bioorganic Phosphorous Chemistry and Chemical Biology (Ministry of Education), Department of Chemistry, Tsinghua University, Beijing 100084, China, [§]Department of Chemistry, Binghamton University, State University of New York, Binghamton, New York 13902, and [¶]Beijing Institute for Brain Disorders, Beijing 100069, China

Edited by Paul E. Fraser

Polymorphism of amyloid-β (Aβ) fibrils, implying different fibril structures, may play important pathological roles in Alzheimer's disease (AD). Morphologies of Aβ fibrils were found to be sensitive to fibrillation conditions. Herein, the Ser^8-phosphorylated Aβ (pAβ), which is assumed to specially associate with symptomatic AD, is reported to modify the morphology, biophysical properties, cellular toxicity, and structures of Aβ fibrils. Under the same fibrillation conditions, pAβ favors the formation of fibrils ($F_{pβ}$), which are different from the wild-type Aβ fibrils ($F_β$). Both $F_β$ and $F_{pβ}$ fibrils show single predominant morphologies. Compared with $F_β$, $F_{pβ}$ exhibits higher propagation efficiency and higher neuronal cell toxicity. The residue-specific structural differences between the $F_β$- and $F_{pβ}$-seeded Aβ fibrils were identified using magic angle spin NMR. Our results suggest a potential regulatory mechanism of phosphorylation on Aβ fibril formation in AD and imply that the post-translationally modified Aβ, especially the phosphorylated Aβ, may be an important target for the diagnosis or treatment of AD at specific stages.

Amyloid fibrils are β-sheet-enriched fibrillar aggregates with misfolded polypeptides and proteins. The formation and deposition of these fibrils are related to a variety of neurodegenerative diseases, including Alzheimer's disease (AD),[3] Parkinson's disease, and Huntington disease among others (1–4). Amyloid fibrils derived from the same primary sequences of polypeptides or proteins usually show distinct morphologies *in vitro* (5, 6), and the morphologies of fibrils are sensitive to a variety of fibrillation conditions such as temperature (7), agitation (8), salt concentrations (9), surfactant (10), and seeding effects (11). Recent evidence revealed that amyloids can spread through a prion-like mechanism where fibrils seem to play important roles (12–14). Different fibrils with their specific morphologies, reminiscent of prion-like strains, may cause distinct pathological phenotypes and link different structures to the variations in disease transmission and pathology (15–17). Furthermore, fragmentation of fibrils, which always produces new ends for self- or cross-seeded fibrillation, is of critical importance for infectious amyloids (18, 19).

Senile plaques consisting of fibrillar Aβ are considered one of the important hallmarks in AD (20). The 40-residue and 42-residue Aβ peptides (*i.e.* Aβ40 and Aβ42, respectively) are the two main fibrillar species. Recently, Aβ has also been reported to exhibit prion-like propagation properties (21, 22). Distinct strains of Aβ were discerned in Alzheimer's patients (23–26). Different amyloid propagation properties and structural profiles of Aβ40 and Aβ42 mimic distinct amyloid strains (10, 27). The phenotypes induced by exogenous injection of Aβ-containing brain extracts from Alzheimer's patients were dependent on both the hosts and the sources of agents, suggesting that polymorphic Aβ strains might result in varying biological activities (25, 28, 29). Molecular structures of Aβ fibrils derived from Alzheimer's patients with distinct clinical histories were also different (24). This underlines that the structural variations of Aβ fibrils may correlate with the variations of pathological phenotypes (24). In addition, compared with the brain-derived Aβ fibrils, the synthetic fibrils showed lower prion activities and different molecular structures (23, 24, 30), implying that some crucial factors *in vivo* might account for different fibrillar polymorphisms and pathological phenotypes.

Recently, post-translational modifications of Aβ, such as phosphorylation and pyroglutamation, occurring *in vivo* have been found to promote the progression of AD (31, 32). Among different types of post-translational modifications, the phosphorylation of proteins plays crucial roles in protein folding (33). Phosphorylation can alter the structures of a protein and modulate its activities (33). Using Trp-cage as a model protein, Kardos *et al.* (34) reported that phosphorylation could serve as a

* This work was supported by Major State Basic Research Development Program of China Grant 2013CB910700, National Natural Science Foundation of China Grants 21472109 and 81661148047, a start-up fund from Binghamton University (to W. Q.), and National Science Foundation Major Research Instrumentation Grant 0922815. The authors declare that they have no conflicts of interest with the contents of this article.

[1] To whom correspondence may be addressed: Binghamton University, SUNY, B28B, Science II, 4400 Vestal Pkwy. East, Binghamton, NY 13902-6000. Tel.: 607-777-2298; Fax: 607-777-4478; E-mail: wqiang@binghamton.edu.

[2] To whom correspondence may be addressed: Tsinghua University, Dept. of Chemistry, Rm. 331, New Life Science Bldg., Beijing 100084, China. Tel.: 86-10-62796197; Fax: 86-10-62781695; E-mail: liym@mail.tsinghua.edu.cn.

[3] The abbreviations used are: AD, Alzheimer's disease; Aβ, amyloid-β; Aβ(3pE)40, Glu^3-pyroglutamated Aβ40; pAβ, Ser^8-phosphorylated Aβ; MAS, magic angle spinning, TEM, transmission electron microscopy; XRD, X-ray diffraction; CIP, calf intestinal alkaline phosphatase; MTT, 3-(4-,5-dimethylthiazol-2-yl)-2,5-diphenyltetrazolium bromide; ThT, thioflavin T; Tricine, *N*-[2-hydroxy-1,1-bis(hydroxymethyl)ethyl]glycine; Fmoc, *N*-(9-fluorenyl)methoxycarbonyl; HFIP, hexafluoroisopropanol; ddH_2O, double distilled H_2O.

conformational switch to trigger the transition from native to amyloid state. Significantly, we and other groups have demonstrated that phosphorylation is involved in the formation of low barrier hydrogen bond (35) and turn conformations (36) as well as the destabilization of β-hairpin structure (37). Furthermore, we have also reported that phosphorylation may modulate the fibrillation process of amyloid proteins, such as Tau and α-synuclein (38–40). Herein, we describe a novel regulatory function of phosphorylation at Ser^8 on morphology, biophysical properties, cellular toxicity, and structures of the Aβ40 fibrils.

It has been shown that phosphorylation at Ser^8 in Aβ has important roles in late onset sporadic AD (31, 41, 42). Phosphorylation at Ser^8 was found in the brains of Alzheimer's patients in a hierarchical sequence and was specially suggested to be associated with symptomatic AD (43). Phosphorylation at Ser^8 was modulated by protein kinase A (44). Additionally, this site-specific phosphorylation was known to accelerate the nucleation-dependent fibrillation of Aβ and to enhance the Aβ-mediated amyloid toxicity (44). Attenuation of Aβ clearance via insulin-degrading enzyme and angiotensin-converting enzyme induced by this phosphorylation was also reported (45). Furthermore, the phosphorylation at Ser^8 could elevate numbers of strong hydrogen bonds in the N terminus of Aβ and increase the stability of the resulting pathogenic fibrils. The latter represents one of the crucial factors for disease progression in the brain (46). Despite all the functional importance, it is not clear whether this residue-specific phosphorylation can modify the morphologies and structures of Aβ fibrils, which are closely related to transmission and progression of AD.

Our present study demonstrates that Aβ40 with phosphorylation at Ser^8 (pAβ) leads to a cross-β fibril ($F_{pβ}$) morphologically and structurally different from the wild-type Aβ fibril ($F_β$). The $F_{pβ}$ and $F_β$ show distinct single predominant morphologies and structures and have different biophysical properties and cellular toxicities. Residue-specific structural variations between the $F_{pβ}$- and $F_β$-seeded 40-residue Aβ fibrils were determined using magic angle spinning (MAS) NMR spectroscopy. Our results show the effects of post-translational modifications on the polymorphism of Aβ fibrils and their potential correlations to the propagation properties and cellular toxicities of the fibrils. Phenomena of strains related to distinct amyloid polymorphism are the subject of extensive interest because of their correlation with different pathological phenotypes (10, 25, 26, 47, 48). The current study also strongly suggests the potential relationship between post-translational modifications and strain formation *in vivo*.

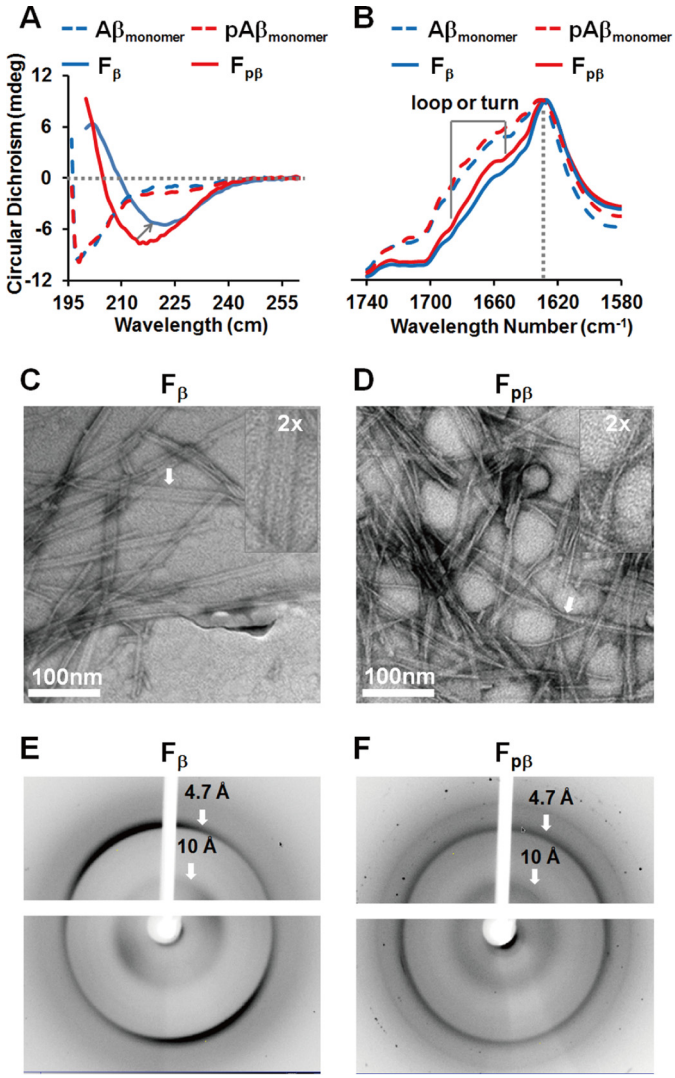

FIGURE 1. **Phosphorylation induces pAβ misfolding into amyloid fibril morphology ($F_{pβ}$) distinct from wild-type Aβ ($F_β$).** *A*, CD spectra of unaggregated Aβ monomers (*blue dashed line*), pAβ monomers (*red dashed line*), $F_β$ fibrils (*blue solid line*), and $F_{pβ}$ fibrils (*red solid line*). Both unaggregated Aβ and pAβ monomers mainly showed similar random coil structures (198 nm). $F_β$ and $F_{pβ}$ fibrils showed β-sheet-enriched structures with a minimum peak at about 222 and 216 nm, respectively. *B*, FT-IR absorbance spectra of unaggregated Aβ monomers (*blue dashed line*), pAβ monomers (*red dashed line*), $F_β$ fibrils (*blue solid line*), and $F_{pβ}$ fibrils (*red solid line*). Both unaggregated Aβ and pAβ monomers showed a symmetrical FT-IR spectrum with a maximum absorbance peak at 1653 cm^{-1}. The $F_β$ and $F_{pβ}$ fibrils showed the same maximum absorbance peak at 1628 cm^{-1} but small variations between 1640 and 1680 cm^{-1} that imply certain structural differences. *C* and *D*, TEM images of $F_β$ fibrils (*C*) and $F_{pβ}$ fibrils (*D*). $F_{pβ}$ exhibited a twisted cylindrical structure, whereas $F_β$ displayed a ribbon-like structure. *E* and *F*, XRD images of $F_β$ fibrils (*E*) and $F_{pβ}$ fibrils (*F*). The reflections at 4.7 and 10 Å, respectively, indicated that both $F_{pβ}$ and $F_β$ fibrils were rich in cross-β structures. *mdeg*, millidegrees.

Results

The $F_{pβ}$ Fibrils Have Different Morphologies Compared with the $F_β$ Fibrils—The $F_β$ and $F_{pβ}$ fibrils were prepared using the same conditions with the same initial peptide concentration at 40 μM. Circular dichroism (CD) and Fourier transform infrared (FT-IR) spectroscopy were first used to study the structures of both monomers and fibrils. Fig. 1, *A* and *B*, shows that CD and FT-IR spectra of the unaggregated monomers of the wild-type Aβ40 and pAβ were very similar. The CD spectra (Fig. 1*A*) suggested that both monomeric Aβ40 and pAβ had mainly random coil structures. Furthermore, the FT-IR spectra (Fig. 1*B*) for both monomeric Aβ40 and pAβ were symmetric from 1580 to 1740 cm^{-1} with maximum peaks at about 1653 cm^{-1}. Interestingly, we observed obvious differences in CD spectroscopy between the $F_{pβ}$ and $F_β$ fibrils. The CD spectra of $F_{pβ}$ and $F_β$ had minimum peaks at about 216 and 222 nm, respectively (Fig. 1*A*), indicating different β-sheet structures in their fibril cores (7, 49, 50). Compared to the $F_{pβ}$ fibrils, the fibrillation of $F_β$ was accompanied by a reduction of CD spectral intensity presumably due to the increased scattering (50). Transmission electron microscopy (TEM) showed that the morphologies of both $F_{pβ}$

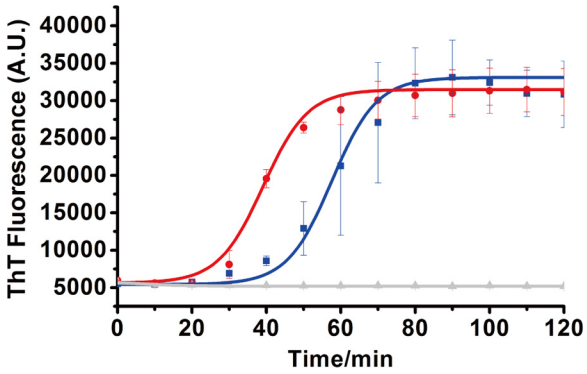

FIGURE 2. **ThT fluorescence kinetic curves of pAβ and Aβ.** For ThT fluorescence kinetics measurements, both 40 μM pAβ (*red*) and Aβ (*blue*) were used and replicated three times with 20 μM ThT in the presence of 20 mM Tris·HCl buffer, 150 mM NaCl, pH 7.4, with continuous shaking. The curves (*solid curves*) were fitted using a sigmoidal equation (50). *Error bars* (S.D.) were calculated from three independent experiments. *A.U.*, arbitrary units.

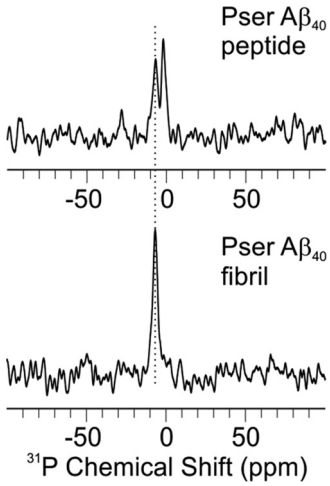

FIGURE 3. **^{31}P MAS NMR spectra for pAβ peptides (*top*) and fibrils (*bottom*).** Both spectra were acquired with 1024-scan signal averaging and processed with 10-Hz Gaussian line broadening.

and F_β fibrils were homogenous. The $F_{p\beta}$ fibrils were mainly twisted cylindrical structures (Fig. 1*D*), which were distinct from the flat ribbon-like morphology for F_β fibrils (Fig. 1*C*). Additionally, the FT-IR spectra (Fig. 1*B*) and X-ray diffraction (XRD) diffraction patterns (Fig. 1, *E* and *F*) revealed that both $F_{p\beta}$ and F_β fibrils were rich in cross-β structures. The FT-IR spectra of both F_β and $F_{p\beta}$ fibrils showed main peaks at $\sim$ 1628 nm^{-1} that were also consistent with previous studies on Aβ fibrils (51–53). However, two spectra were distinct in the loop or turn regions between 1640 and 1680 cm^{-1}, indicating certain levels of structural variations between the two fibrils. The XRD pattern showed reflections at 4.7 and 10 Å for the inter- and intramolecular spacing, respectively, which characterized the cross-β structures for both F_β and $F_{p\beta}$ fibrils (54). Taken together, we found that phosphorylation of Aβ40 at Ser^8 could modify the morphologies of amyloid fibrils. Recent evidence has shown that different microenvironments modulate the free energy landscapes for Aβ folding into different morphological states (8, 25, 50). It is possible that the side-specific phosphorylation may alter the free energy barrier for the folding of Aβ40 and lead to a different morphology for the pAβ.

Phosphorylation Plays Crucial Roles in $F_{p\beta}$ Formation—Recently, Rezaei-Ghaleh *et al.* (46, 55) have shown that phosphorylation at Ser^8 could impel the undergoing changes in local conformational dynamics of Aβ40, induce the variations of N-terminal exposure of Aβ aggregates, and increase the fibril stability by promoting the formation of strong hydrogen bonds directly. We propose that different conformations of $F_{p\beta}$ fibrils may also be induced directly by phosphorylation. The thioflavin T (ThT) fluorescence kinetics measurement was first applied to determine the fibrillation rate of pAβ. ThT fluorescence kinetics measurements of 40 μM monomeric Aβ40 and pAβ were conducted at 37 °C with continuous shaking. Both Aβ40 and pAβ exhibited typical nucleation-dependent sigmoidal curves (Fig. 2). Similar to previous results from Kumar *et al.* (44), phosphorylation at Ser^8 accelerated the fibrillation process (Fig. 2). The lag times of fibrillation for 40 μM pAβ and Aβ40 were 22 and 38 min, respectively. Furthermore, pAβ seemed to decrease the aggregation half-time (39.1 $\pm$ 9.0 min) compared with Aβ40 (57.6 $\pm$ 13.2 min). These results suggested that phosphorylation might either shorten or alter the fibrillation process of Aβ.

Solid-state ^{31}P NMR spectra for the $F_{p\beta}$ fibrils and the monomeric pAβ peptides are shown in Fig. 3. Both spectra were recorded with similar quantities of samples ($\sim$8 mg) and the same hydration level ($\sim$1 μl/mg). The direct polarization ^{31}P spectroscopy allowed quantitative comparison of the peak intensities between the two samples. The fact that the ^{31}P intensity was greatly enhanced in the $F_{p\beta}$ sample suggested that the phosphate group at Ser^8 was located in an ordered environment upon fibrillation compared with the monomeric peptides. Furthermore, different from the monomeric pAβ sample, which might form amorphous aggregates because of the rehydration, the fibrillar $F_{p\beta}$ ^{31}P spectrum showed only one predominant peak, suggesting a single local conformation for the side chain of Ser^8.

To further uncover the roles of phosphorylation in $F_{p\beta}$ fibrils, the alkaline phosphatase dephosphorylation assay was applied (56). We utilized calf intestinal alkaline phosphatase (CIP) purified from calf intestinal mucosa that can remove phosphate groups from phosphorylated species (57). Previous work has suggested the involvement of phosphorylated Ser^8 in specific hydrogen bonding to the hydrophobic core of fibrils (46, 55). In these cases, the phosphate group might be restricted, and efficiency of dephosphorylation might decrease. In our experimental design, the monomeric pAβ (Fig. 4, *A* and *C*) and $F_{p\beta}$ fibrils (Fig. 4*B*) were treated with a series of CIP solutions with different enzymatic concentrations for 30 min, and then the dephosphorylated pAβ bands were traced using Tricine-SDS-PAGE (Fig. 4, *A* and *B*) and native PAGE (Fig. 4*C*). Only Tricine-SDS-PAGE was used to trace the bands after dephosphorylation of fibrils (Fig. 4*B*) because fibrils could not be disassociated and enter into the gel in native PAGE. The results showed that dephosphorylation of pAβ generated Aβ40 in a concentration-dependent manner. Furthermore, the phosphate groups on Ser^8 in monomeric pAβ could be cleaved by CIP much more easily than those in $F_{p\beta}$ fibrils (Fig. 4, compare the corresponding bands in *A* with those in *B*). Even at a lower concentration of CIP (0.1 unit of CIP enzymatic activity), monomeric pAβ was

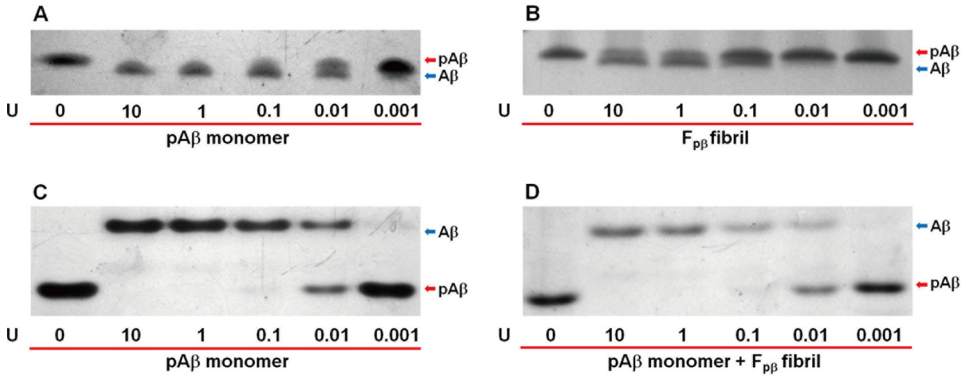

FIGURE 4. **Dephosphorylation of pAβ monomers (*A* and *C*), $F_{p\beta}$ fibrils (*B*), and pAβ monomers mixed with equal moles of $F_{p\beta}$ fibrils (*D*).** The pAβ monomers (*A* and *C*), $F_{p\beta}$ fibrils (*B*), or pAβ monomers mixed with equal moles of fibrils (*D*) were incubated with a series of CIP concentrations in 20 mM Tris·HCl buffer, 150 mM NaCl, pH 7.4, and traced using 12% Tricine-SDS-PAGE (*A* and *B*) and native PAGE (*C* and *D*), respectively. Enzymatic activity of CIP is shown at the *bottom* of the gel where *U* is the unit of CIP enzymatic activity. Dephosphorylation of pAβ monomers or $F_{p\beta}$ fibrils could generate Aβ in a concentration-dependent manner. Comparison of the dephosphorylation of $F_{p\beta}$ fibrils (*B*) with pAβ monomers (*A*) showed that fibril formation could clearly limit dephosphorylation partially. The same dephosphorylation trends of pAβ monomers in the absence (*C*) or presence (*D*) of $F_{p\beta}$ fibrils were observed. These results showed that the presence of $F_{p\beta}$ fibrils did not influence the enzymatic activity of CIP. The *upper* and *lower* protein bands in *A* and *B* (Tricine-SDS-PAGE) denote pAβ and Aβ, respectively. The *upper* and *lower* protein bands in *C* and *D* native PAGE) denote Aβ and pAβ, respectively.

almost completely dephosphorylated. For $F_{p\beta}$ fibrils, however, the phosphate groups were only partially removed even at high CIP concentrations, such as 1 and 10 units of CIP enzymatic activity (*i.e.* Fig. 4, two bands for both pAβ and Aβ in *B*, *second* and *third columns*, compared with only a single band for Aβ in the corresponding columns in *A*). Therefore, we identified that $F_{p\beta}$ fibril formation clearly limited the dephosphorylation by CIP. Recently, evidence has shown that fibrils can sequester different kinds of proteins and change their corresponding physiological properties (58, 59). Fibrils might also influence the enzymatic activities (60, 61). Therefore, dephosphorylation of pAβ monomers mixed with equal moles of $F_{p\beta}$ fibrils (native PAGE in Fig. 4*D*) was tested to exclude the possibility that fibrils might trap the CIP and lower the enzymatic activity. Only native PAGE was used to identify the new bands after dephosphorylation because the bands from disrupted fibrils in SDS-PAGE would influence the results. Comparison of Fig. 4, *C* and *D*, showed that the presence of $F_{p\beta}$ fibrils did not affect the enzymatic activity of CIP because the dephosphorylation effects of this enzyme on pAβ monomers were similar both in the absence (Fig. 4*C*) and presence (Fig. 4*D*) of fibrils. Collectively, these results suggest that the phosphorylation at Ser^8 would directly induce the formation of certain structures in $F_{p\beta}$ fibril.

$F_{p\beta}$ and F_β Fibrils Show Distinct Propagation Activities and Cellular Toxicities—Distinct fibril morphologies have been considered to affect the symmetries and lateral association propensities of protofilaments (8). Consequently, the morphological differences between $F_{p\beta}$ and F_β fibrils might imply their structural diversities, such as the surface exposure of different amino acid side chains, which might further be correlated with prion-like propagation (30, 48) and cellular toxicities (8, 9), etc.

First, the prion-like propagation of $F_{p\beta}$ and F_β fibrils *in vitro* was monitored by a ThT fluorescence assay on the seeded fibrillation (62), and TEM was used to examine the structural natures of aggregates after seeding. Both $F_{p\beta}$ and F_β fibrils were sonicated in an ice bath to produce small fragments (Fig. 5). The wild-type Aβ40, Aβ42, and pyroglutamated Aβ3–40, which is an important post-translationally modified form of Aβ (named Aβ(3pE)40 hereinafter) (63), were tested on the cross-seeding efficiencies for the seeds of $F_{p\beta}$ and F_β fibrils. Fig. 6*A* plots the ThT kinetics curves of Aβ40 in the presence of 10% $F_{p\beta}$ and F_β seeds. Both seeds greatly shortened the lag phase, and $F_{p\beta}$ initiated the fibrillation more rapidly compared with the F_β-seeded fibrillation. The significant difference in the lag time between the $F_{p\beta}$- (almost no lag time) and F_β-seeded fibrillation (296 min) is shown in Fig. 6*D*. We emphasize that the results in Fig. 6*A* suggested that the wild-type Aβ40 formed fibrils more rapidly in the presence of $F_{p\beta}$ seeds in comparison with its own seeds, meaning that the cross-seeding between pAβ and wild-type Aβ40 was more efficient than the self-seeding of wild-type Aβ40. Interestingly, we found that the ThT intensities of seeded plateaus in Fig. 6*A* were lower than that of unseeded. The concentrations of Aβ40 in both the parental and seeded fibrils were 40 μM. Therefore, the intensity difference was not likely to originate from the quantities of fibrils. We postulated that the ThT fluorescence intensity was reduced in seeded fibrils because certain fibril structures with low ThT fluorescence emission were selectively amplified during the seeding process as has been suggested by a previous work from Tycko and co-workers (64). Fig. 6, *B* and *C*, further show that, for the Aβ(3pE)40 and wild-type Aβ42, the $F_{p\beta}$ induced more efficient cross-seeding than the wild-type F_β. Overall, our results suggested that the pAβ (*i.e.* Ser^8-phosphorylated Aβ40) might serve as an intrinsic trigger to promote the fibrillation of a variety of Aβ species. As revealed by TEM, both the Aβ40 and Aβ(3pE)40 fibrils seeded from $F_{p\beta}$ showed similar twist-like morphologies (Fig. 6, *G* and *H*, *right panel*), whereas the Aβ40 and Aβ(3pE)40 fibrils seeded from F_β showed ribbon-like morphologies (Fig. 6, *G* and *H*, *left panel*). These results indicated that both $F_{p\beta}$ and F_β fibrils could propagate their structures to Aβ40 and Aβ(3pE)40. However, under the same seeding conditions, although the fibrillation times were significantly shortened, a similar morphology was obtained for both $F_{p\beta}$- and F_β-seeded Aβ42 fibrils (Fig. 6*I*) that was different from either the parental $F_{p\beta}$ or F_β fibrils. It was proposed previously that the seeded fibrillation process involves mainly chain elongation from the existing structural patterns of the seeds (65). For Aβ40

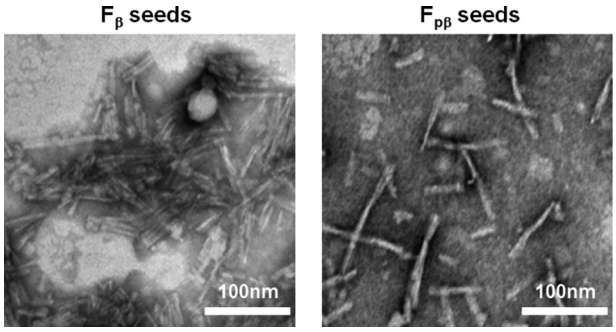

FIGURE 5. **TEM images of sonicated seeds of F_β and $F_{p\beta}$.** Both Aβ (*left*) and pAβ (*right*) seeds were produced by sonicating the F_β and $F_{p\beta}$ fibrils, respectively, in the ice bath three times (for 1.5 min each time).

and Aβ(3pE)40, it was interesting that the $F_{p\beta}$ seeds served as a better structural template for the Aβ chain elongation compared with F_β seeds, which would reflect the differences in the intrinsic architectures of the two fibrils. The conformational transition from partially folded Aβ to β-sheet-enriched state is an essential process for Aβ aggregation, and the seeded fibrillation might follow the "docking conformational change" mechanism in which the existence of fibril seeds as templates would lower the "activation energy" for the conformational switch (66–68). The differences of the fibrillation process in the presence of the F_β and $F_{p\beta}$ seeds revealed that phosphorylated fibrils possibly contained the core structures that would decrease the energy barrier and promote the efficiency of chain elongation much more easily. Surprisingly, despite the high similarity of the Aβ40 and Aβ42 sequences, monomeric Aβ42 was incompatible with the structural nature of either F_β or $F_{p\beta}$ seeds. Although the shortened lag time was detected when Aβ42 was seeded by both $F_{p\beta}$ and F_β fibrils, the resulting Aβ42 fibrils did not inherit the parental structural information. This implies that Aβ42 cannot be directly converted to fibrils at the termini of the seeds of $F_{p\beta}$ and/or F_β fibrils by using the structural template from seeds. A similar phenomenon was also observed in a previous study of α-synuclein strains (9). One possible explanation was that the $F_{p\beta}$ and F_β seeds only served as a "surface" to catalyze the formation of fibrils but not as structural templates.

To explore whether the $F_{p\beta}$ fibrils possessed different levels of cytotoxicity compared with the wild-type F_β fibrils, both fibrils were applied extracellularly to mouse neuroblastoma N2a cells and mouse microglia BV-2 cells. The cell viabilities were investigated using 3-(4-,5-dimethylthiazol-2-yl)-2,5-diphenyltetrazolium bromide (MTT) assay (Fig. 7). After 24-h treatment, both fibrils showed concentration-dependent cytotoxicities to these two mammalian cells. The twisted $F_{p\beta}$ fibrils showed significantly higher cytotoxicity than the flat ribbon F_β fibrils. Ribbon-like and twisted fibrils are two major types of fibril morphologies formed by amyloid proteins, including Aβ (8, 69, 70), amylin (71), and α-synuclein (9), depending on the growth conditions. Different fibril structures have been shown to correlate with distinct morphologies and different levels of concentration-dependent cytotoxicities (6, 69). We observed higher toxicity for the twisted $F_{p\beta}$ fibrils compared with the ribbon-like F_β fibrils, which was consistent with the potential correlation between morphology and cytotoxicity observed in other Aβ and α-synuclein fibrils (8, 9). We suspect that different lateral association and symmetry of twisted and ribbon-like morphologies might lead to distinct packing geometries and different exposures of residues on the fibril surface and therefore might induce different levels of toxicity to cells.

Molecular Structural Differences between the $F_{p\beta}$- and F_β-seeded Aβ40 Fibrils—Given the differences in the fibril morphologies, biophysical characterizations, and cytotoxicities, we were interested in whether there are molecular level structural variations between the $F_{p\beta}$ and F_β fibrils. This was done by MAS NMR studies on the $F_{p\beta}$- and F_β-seeded Aβ fibrils. The seeded fibrils were prepared by adding 10% $F_{p\beta}$ or F_β seeds to freshly dissolved 40 μM Aβ40 monomers followed by quiescent incubation for 48 h under physiological temperature and pH. This protocol minimized the manipulations on fibrillar structures and was likely to produce seeded fibrils that were similar to their parents (8, 72). We verified the structural similarity using TEM and CD spectroscopy and examined the cytotoxicities of daughter fibrils using the MTT assay (Fig. 8). The CD spectra showed minimum peaks at 216 and 222 nm for the $F_{p\beta}$- and F_β-seeded fibrils, respectively (Fig. 8*A*), that were identical to their parent fibrils. In Fig. 8*B*, the TEM images show that the features for the $F_{p\beta}$ and F_β fibrils, which were the twisted cylindrical and flat ribbon-like morphologies, respectively, were propagated to their daughter fibrils. In Fig. 8*C*, we found that daughter fibrils from both F_β and $F_{p\beta}$ seeds showed concentration-dependent cytotoxicities to the two mammalian cells. Daughter fibrils seeded from $F_{p\beta}$ also showed higher cytotoxicity where the trend was similar to that of their parental fibrils. Therefore, we concluded that $F_{p\beta}$- and F_β-seeded fibrils would retain structural characteristics from their parental fibrils.

Extensive MAS NMR measurements were performed to probe the residue-specific secondary structures of both seeded fibrils. We used six scattering uniformly isotope-labeled Aβ peptides to cover the majority of the primary sequence, especially the typical β-strands and interstrand loop segments from the known Aβ fibril structures (24, 27, 69, 73–75). Representative NMR spectra and the summary of chemical shift deviations are plotted in Fig. 9. The chemical shift assignments for both seeded fibrils are provided in Tables 1 and 2. Overall, both fibrils showed typical β-loop-β structures like other known 40-residue Aβ fibrils. However, detailed structural variations were observed. First, the local secondary structure of Gly^9, which is next to the phosphorylated Ser^8, changed significantly. The wild-type F_β fibrils showed multiple Gly^9 C′-Cα cross-peaks, whereas the phosphorylated $F_{p\beta}$ fibrils had a predominant cross-peak (Fig. 10*A*). This observation was consistent with the ^{31}P NMR (Fig. 3) and confirmed that the local conformation around Ser^8 became better defined due to the phosphorylation. Second, the site-specific phosphorylation affected not only the local conformation but also the overall secondary structures of the resulting fibrils. As shown in Fig. 9, we identified significant chemical shift deviations between the $F_{p\beta}$ and F_β fibrils, and the largest chemical shift differences were observed for residues Gly^9, the segments between Leu^{17} and Ile^{32}, and the residue Val^{39}. Particularly, the segments Asp^{23}–Ser^{26} and Gly^{29}–Ile^{32} showed the most significant chemical shift deviations between the two fibrillar species. The C-termi-

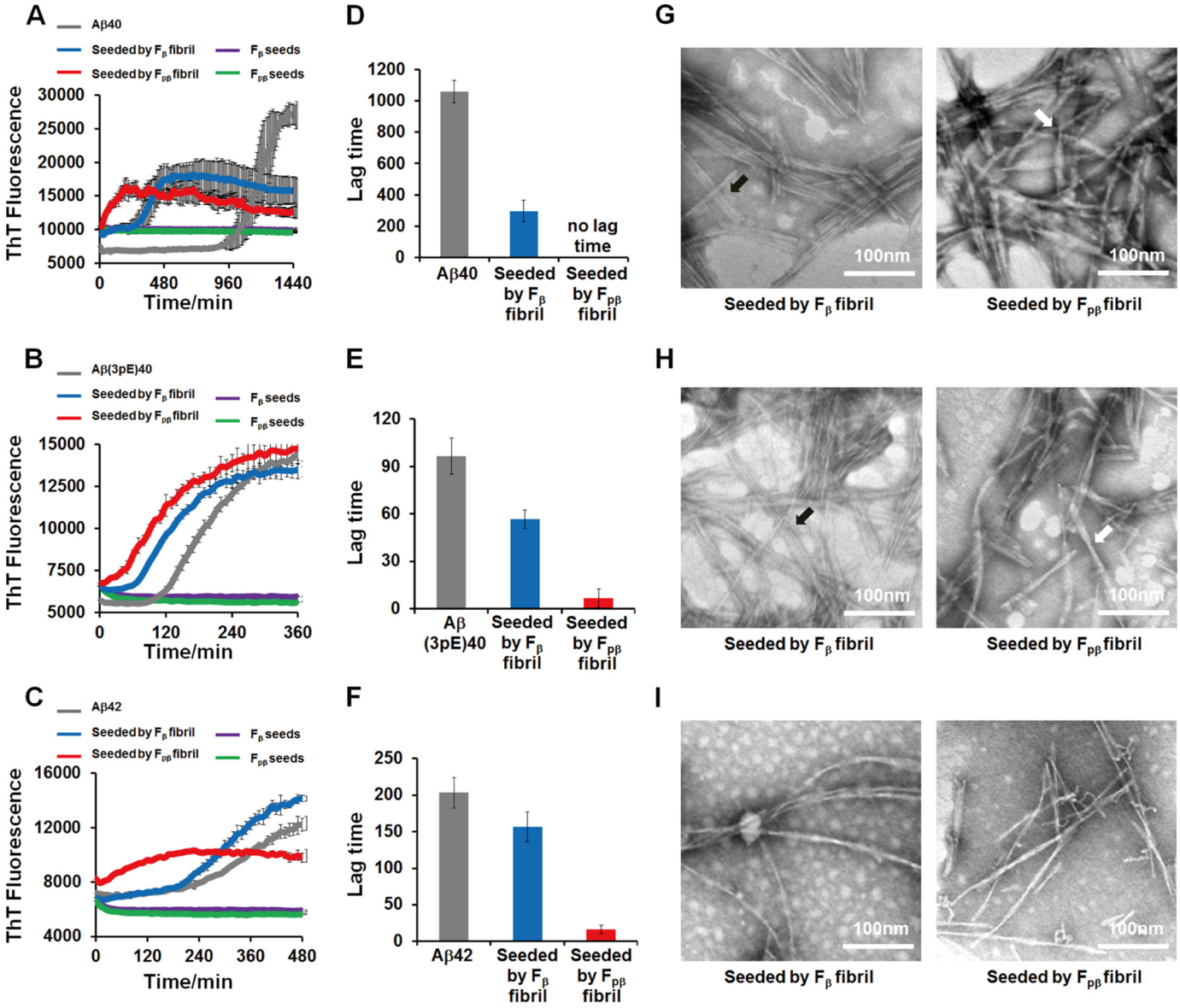

FIGURE 6. **Propagation of $F_{p\beta}$ and F_{β} fibrils *in vitro* was monitored by ThT kinetics assay and TEM images.** Propagation of preformed 10% $F_{p\beta}$ (*red curves*) and F_{β} fibrils (*blue curves*) in 40 μM Aβ40 (*A*), 10 μM Aβ(3pE)40 (*B*), and 10 μM Aβ42 (*C*) *in vitro* at pH 7.4 was monitored by ThT fluorescence kinetics assay. The lag phase for Aβ40 (*D*), Aβ(3pE)40 (*E*), and Aβ42 (*F*) showed that both $F_{p\beta}$ (*red column*) and F_{β} (*blue column*) can shorten the lag phase for amyloid formation. The structural natures of Aβ40, Aβ(3pE)40, and Aβ42 aggregates after seeding were examined using TEM (*G*, *H*, and *I*, respectively); *left* and *right panels* are structural images of F_{β}-seeded fibrils and $F_{p\beta}$-seeded fibrils, respectively. The TEM samples were prepared after 24-h incubation. For Aβ40 (*G*) and Aβ(3pE)40 (*H*), the structural information of parental F_{β} fibrils and $F_{p\beta}$ fibrils can be inherited. The *black* and *white arrowheads* point to ribbon-like and twisted cylindrical morphologies, respectively. However, Aβ42 cannot sample the structural information from either F_{β} or $F_{p\beta}$ fibrils (*I*). ThT fluorescence kinetics of different soluble Aβ species without any seeds and F_{β} or $F_{p\beta}$ seeds only were also conducted as controls. *Error bars* represent S.E. ($n = 3$ independent measurements).

nal β-strand region from Gly^{33} to Gly^{38}, in contrast, seemed to have little structural variation. Additionally, it seemed that the $F_{p\beta}$ fibrils had more ordered C termini compared with the F_{β} fibrils because the Val^{39} cross-peaks were much stronger in the $F_{p\beta}$-seeded fibrils then in the F_{β}-seeded fibrils (Fig. 10, *B* and *C*). Importantly, the segment between Ala^{21} and Ala^{30} is generally considered as the interstrand loop region based on the known 40-residue Aβ fibril structures and might be involved in the early stages of fibrillation according to previous studies on Aβ and other similar types of amyloid peptides (76, 77). Because the seeded fibrils were likely to have the same structures as their parents, our results suggested that the phosphorylation on Ser^{8} might affect the intermediate Aβ structures formed during the nucleation steps through specific molecular interactions between the phosphorylated Ser^{8} side chains and residues located in the loop segment between Ala^{21} and Gly^{29}. Interestingly, recent work (46) showed that the phosphorylation of Ser^{8} stabilized the Aβ fibrils through a potential inter-residue interaction among Asp^{7} and the phosphorylated Ser^{8} and Ser^{26}, which was consistent with our NMR data.

Discussion

In this decade, polymorphic Aβ fibrils with different neuronal cytotoxicities and propagation efficiencies have attracted intense attention (6). Small variations of microenvironments *in vitro* will change the kinetics and thermodynamics for aggrega-

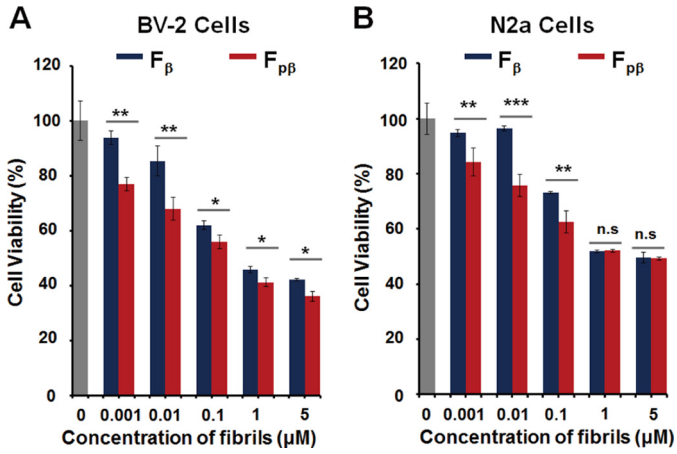

FIGURE 7. **Cytotoxicity of $F_{p\beta}$ and F_β fibrils were measured using MTT assay.** Cell viability of BV-2 cells (*A*) and N2a cells (*B*) treated with F_β and $F_{p\beta}$ fibrils, respectively, for 24 h was measured using an MTT assay. The blank control is shown in *gray columns*. $F_{p\beta}$ fibrils shows higher toxicity compared with F_β fibrils in a concentration-dependent manner. n.s., not significant. S.E. is shown as *error bars* ($n = 3$ independent measurements; *, $p < 0.05$; **, $p < 0.01$; ***, $p < 0.001$ as evaluated with independent Student's *t* test).

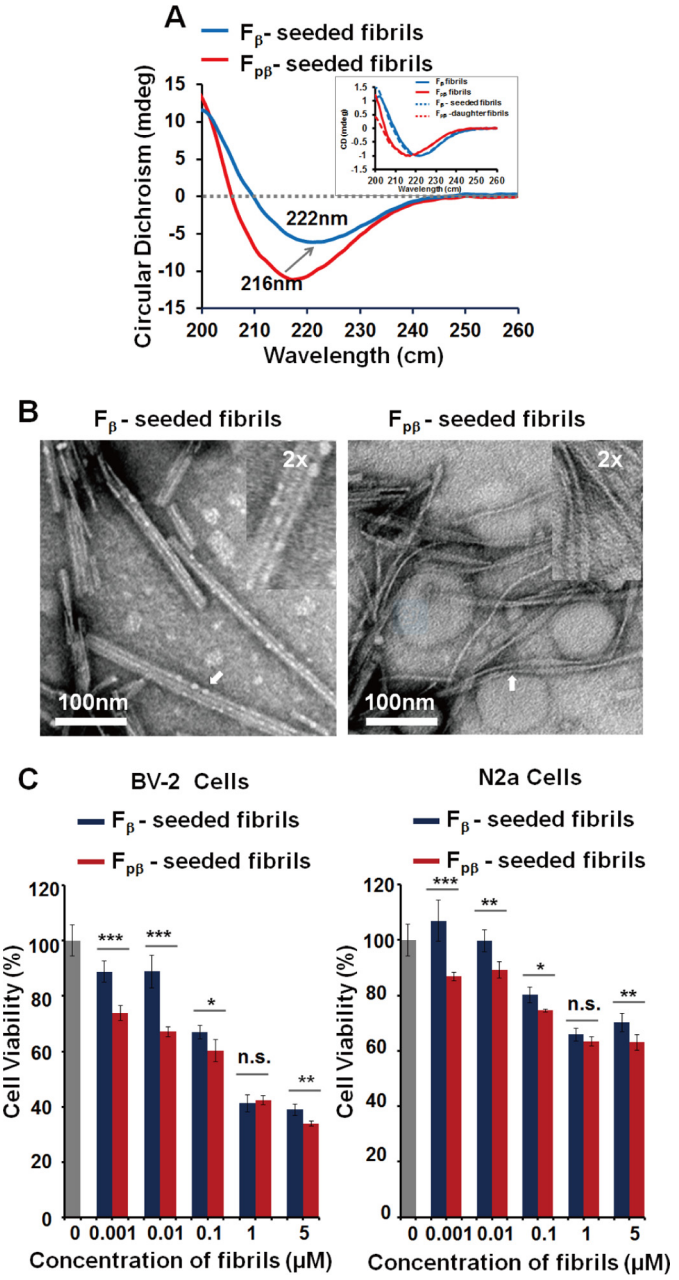

FIGURE 8. **CD spectroscopy, TEM images, and MTT assay indicated that structural features of $F_{p\beta}$ and F_β fibrils could be propagated to their daughter fibrils.** 40 μM Aβ40 was used to examine the structural natures after seeding. *A*, CD spectroscopy showed that the minimum peak of $F_{p\beta}$- and F_β-seeded fibrils was the same as their parent fibrils, respectively. The *inset* is normalized CD spectroscopy curves of parent and daughter fibrils. *B*, TEM images of $F_{p\beta}$- and F_β-seeded fibrils were identical to their parent fibrils. The samples were prepared after 48-h incubation. *C*, MTT assay showed that $F_{p\beta}$-seeded fibrils had higher cytotoxicity of which the trend was the same as for their parental fibrils. S.E. is shown as *error bars* ($n = 3$ independent measurements; *, $p < 0.05$; **, $p < 0.01$; ***, $p < 0.001$; *n.s.*, not significant; as evaluated with independent Student's *t* test). *mdeg*, millidegrees.

tion (8, 70). This may be induced by the coexistence of multiple nucleation processes, each of which favors its own fibril structures (78). Morphological differences induced by variations in fibrillation conditions imply that experimentally based microenvironments (agitation, pH, ionic strength, etc.) may lead to a favorable nucleation process (8, 9, 50, 69, 70, 78). For Aβ40 fibrils, two major types of fibrillar morphologies have been reported. One is the twisted filament with a 3-fold molecular symmetry, and the other is the ribbon-like filament with a 2-fold molecular symmetry (8, 69, 70). Herein, we report the effects of phosphorylation at Ser^8, which is an existing post-translational modification of Aβ *in vivo* (42, 43), on the fibrillation of Aβ. Similar to the effects of microenvironment variation on amyloid formation, phosphorylation at Ser^8 changes the nucleation process of Aβ and finally leads to fibrils with distinct morphologies. Under the same fibrillation conditions, the pAβ folds into a twisted fibril, and Aβ folds into a flat ribbon-like fibril. The N-terminal post-translational modifications of Aβ, such as phosphorylation (31), pyroglutamation (63), and nitration (79), have been reported to control the kinetic process for Aβ fibrillation, accelerate plaque formation, and alter the prion-like propagation efficiency. We first revealed that phosphorylation at Ser^8, acting as an intrinsic molecular trigger beyond the variations of fibrillation conditions, can induce pAβ folding into different fibril morphologies.

The prion-like strain phenomenon where a single amyloid protein gives rise to multiple distinct phenotypes has been correlated with the ability of some polypeptides or proteins to fold into distinct fibril structures in neurodegenerative disease (16, 17). Aβ seeds have been found to possess a transmission risk like prion protein aggregates *in vivo* (22). Our study herein indicates that phosphorylation results in Aβ fibril morphology distinct from the wild-type Aβ, which proposes a possible intrinsic origin of polymorphous fibrils of Aβ. Neurotoxic studies and seeding experiments show that $F_{p\beta}$ and F_β fibrils from pAβ and wild-type Aβ, respectively, have different cytotoxicities and seeding efficiencies, which probably arise from strain-specific structural variation. The results suggest that phosphorylation may act as a possible factor to induce the formation of strains of Aβ. A recent study by Rijal Upadhaya *et al.* (43) showed that phosphorylation of Aβ occurred in the Alzheimer's brain in a hierarchical sequence and promoted the formation of final toxic aggregates, and this phosphorylation was assumed to be indicative for biochemical Aβ stage 3 and associated with

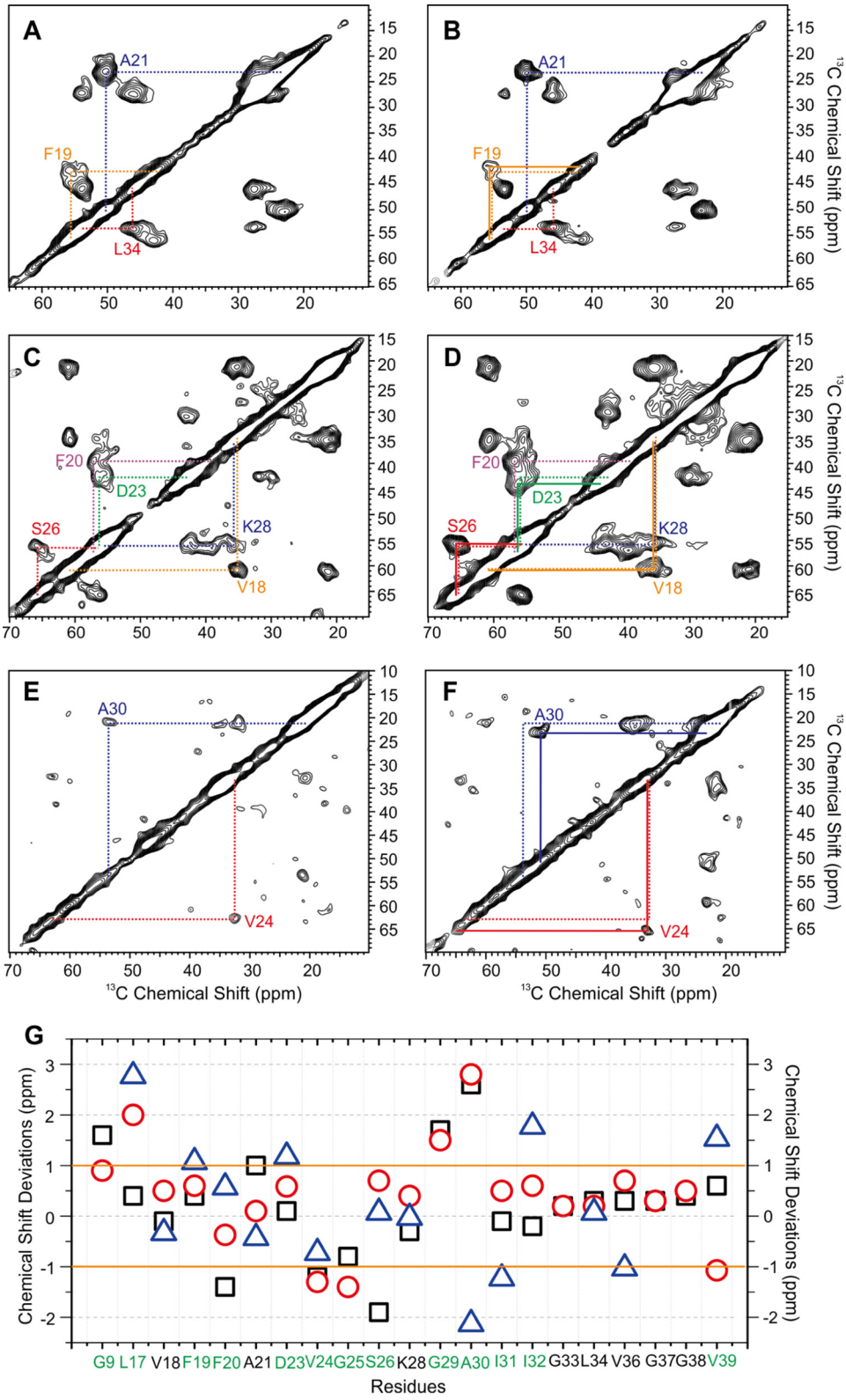

FIGURE 9. **MAS NMR spectra and chemical shift deviations of F_{β}- and $F_{p\beta}$-seeded 40-residue Aβ fibrils.** The $F_{p\beta}$-seeded fibrils (*A*, *C*, and *E*) and F_{β}-seeded fibrils (*B*, *D*, and *F*) were isotope-labeled at different residues. Intraresidual Cα-Cβ cross-peaks are highlighted in *colored lines*. The differences between *dashed* and *solid lines* in *B*, *D*, and *F* indicate shifts in cross-peaks. *G* shows the residue-specific chemical shift deviations ($\delta(F_{p\beta}$-seeded) $-$ $\delta(F_{\beta}$-seeded)) for C′ (*black squares*), Cα (*red circles*), and Cβ (*blue triangles*). The *solid orange lines* highlight the $\pm$1.0-ppm threshold for significant chemical shift deviation based on the estimation of ^{13}C NMR line widths. Residues with at least one significant chemical shift deviation among C′, Cα, and Cβ are highlighted in *green* on the *x axis*.

TABLE 1
^{13}C chemical shifts for the $F_{p\beta}$-seeded fibrils

	C′	Cα	Cβ	Cγ	Cδ	Cε
	ppm	*ppm*	*ppm*	*ppm*	*ppm*	*ppm*
Gly^{9}	172.4	45.4				
Leu^{17}	174.2	54.1	45.8	28.8	24.6	
Val^{18}	172.9	61.1	35.3	21.2		
Phe^{19}	172.4	56.2	42.7			
Phe^{20}	172.8	56.8	39.8			
Ala^{21}	175.4	50.1	22.9			
Asp^{23}	173.9	56.5	43.7	176.2		
Val^{24}	173.8	62.9	32.5	20.7		
Gly^{25}	171.9	44.8				
Ser^{26}	172.3	56.2	65.8			
Lys^{28}	173.6	55.8	35.2	25.5	31	42.6
Gly^{29}	172.7	45.8				
Ala^{30}	176.6	53.4	20.9			
Ile^{31}	174.5	62.2	38.3	27.7	15.6	12.9
Ile^{32}	174.4	59.1	42.3	27	18.9	14.1
Gly^{33}	171	44.9				
Leu^{34}	173.6	53.6	46	27.5	24.6	
Val^{36}	174.4	60.4	34.6	21.6		
Gly^{37}	171.7	47.5				
Gly^{38}	173.5	49.8				
Val^{39}	176	60.4	35.3	21.7		

TABLE 2
^{13}C chemical shifts for the F_{β}-seeded fibrils

	C′	Cα	Cβ	Cγ	Cδ	Cε
	ppm	*ppm*	*ppm*	*ppm*	*ppm*	*ppm*
Gly^{9}	170.8	44.5				
Leu^{17}	173.8	52.1	43	26.2		
Val^{18}	173	60.6	35.8	21.2		
Phe^{19}	172	55.6	41.6			
Phe^{20}	174.2	57.1	39.2			
Ala^{21}	174.4	50	23.3			
Asp^{23}	173.8	55.9	42.5			
Val^{24}	175	64.2	33.2	21.6		
Gly^{25}	172.7	46.2				
Ser^{26}	174.2	55.5	65.7			
Lys^{28}	173.9	55.4	35.2	27.4	30.2	42.5
Gly^{29}	171	44.3				
Ala^{30}	174	50.6	23			
Ile^{31}	174.6	61.7	39.5	28.7	17.4	13.6
Ile^{32}	174.6	58.5	40.5	26.2	16.2	12.1
Gly^{33}	170.8	44.7				
Leu^{34}	173.3	53.4	45.9	27.4	24.8	
Val^{36}	174.1	59.7	35.6	20.7		
Gly^{37}	171.4	47.2				
Gly^{38}	173.1	49.3				
Val^{39}	175.4	61.5	33.7	22.3		

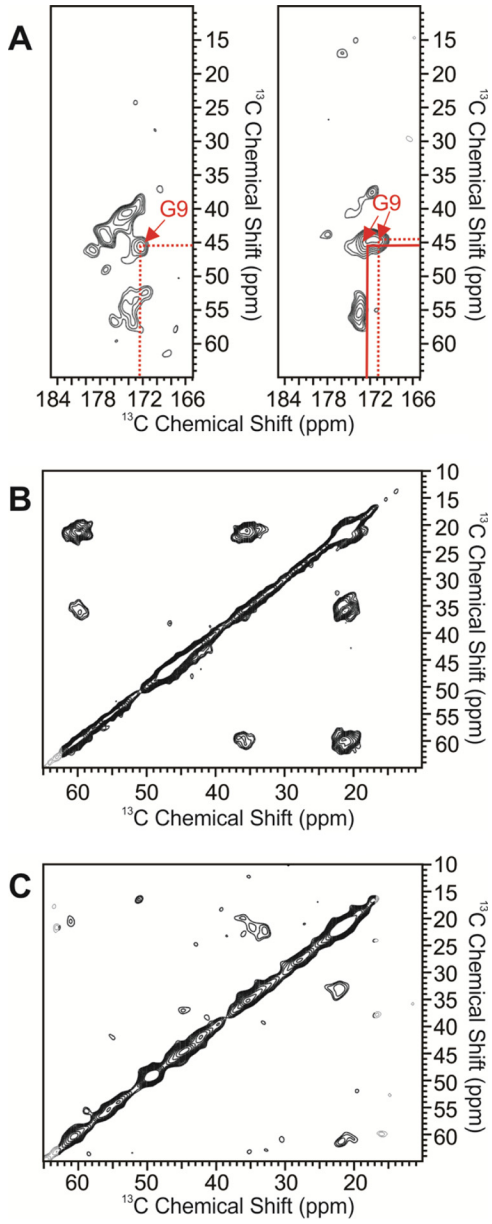

FIGURE 10. **2D ^{13}C-^{13}C MAS NMR spectra.** *A*, cross-peaks for Gly^{9} in $F_{p\beta}$-seeded (*left*) and F_{β}-seeded (*right*) fibrils. *B* and *C*, cross-peaks for Val^{39} in $F_{p\beta}$-seeded (*B*) and F_{β}-seeded (*C*) fibrils.

symptomatic AD. We suggest that the occurrence of phosphorylation was not just an inducer for the further accumulation of total aggregates but might be an initiator for the formation of certain amyloid morphologies with specific biological activities.

Recently, the structures and stabilities of Aβ40 phosphorylated at Ser^{8} have been studied by Rezaei-Ghaleh *et al.* (46, 55) using solution NMR spectroscopy and molecular dynamics simulations. These studies mainly concluded that the phosphorylated Ser^{8} was not included in the fibril core, which typically consisted of residues 15–40. In the monomeric state in solution, the phosphorylation at Ser^{8} mainly affected the local conformation from residues 4 to 16. However, it also promoted the inter-residual interactions between segments Asp^{23}–Gly^{25} and Gly^{29}–Ala^{30}, which are located in the inter-β-strand loop region in Aβ fibrils (55). Combined with our solid-state NMR measurements on the chemical shift differences between $F_{p\beta}$- and F_{β}-seeded fibrils, we propose that the Ser^{8} phosphorylation might affect the initial nucleation of Aβ fibrillation. This site-specific phosphorylation might stabilize certain conformations within the segment Asp^{23}–Ala^{30}, presumably through a transient hydrogen bonding interaction based on the previous molecular dynamics simulation (46). The fact that we observed the most significant chemical shift differences within the segments Asp^{23}–Ser^{26} and Gly^{29}–Ile^{32} between the two types of fibrils further supports the hypothesis. The residues located between two typical β-strands in amyloid fibrils have been proposed as general initial nucleation sites in the fibrillation process of Aβ and other types of amyloid peptides (76, 77). Therefore, stabilization of local conformations in this region might accelerate the rates of nucleation and may lead to different fibril morphology.

In summary, amyloid fibrils together with small aggregates, such as oligomers and protofibrils, are considered important pathological agents in AD. Our study raises the possibility that

different Aβ strains would occur in a phosphorylation-dependent manner. Compared with the wild-type Aβ fibrils, phosphorylation at Ser^8 leads to an overall fibril structural change with significant chemical shift deviations in the segments Asp^{23}–Ser^{26} and Gly^{29}–Ile^{32}. Along with the recent study from Rezaei-Ghaleh *et al.* (46, 55), we propose that the effects of phosphorylation at Ser^8 on the local conformation of residues 4–16 and the inter-residual interactions in the interstrand loop region from residues 21 to 30 would cooperatively promote pAβ to fold with a distinct nucleation process and finally lead to a fibril morphology different from that of wild-type Aβ. Combined with the potential link between phosphorylation and symptomatic AD (43), we propose that pAβ might serve as a specific therapeutic target for AD. The specific link between Aβ strains and phosphorylation raises the possibility of designing structure-based imaging agents and inhibitors to diagnose or prevent AD at different stages.

Experimental Procedures

Sample Preparation—All Aβ peptides with the same primary sequence (DAEFRHDSGYEVHHQKLVFFAEDVGSNKGAIIGLMVGGVV) were prepared using Fmoc chemistry with Fmoc-Val-Wang resin (0.18 mmol/g; GL Biochem (Shanghai) Ltd.). Fmoc-Ser(PO_3Bzl)-OH (where Bzl is benzyl) (GL Biochem (shanghai) Ltd.) and uniformly ^{13}C- and ^{15}N-labeled amino acids (Cambridge Isotope Laboratories, Inc.) were incorporated into the peptides to achieve phosphorylated and isotope-labeled Aβ peptide sequences. The Glu^3-pyroglutamated Aβ40 (Aβ(3pE)40; pEFRHDSGYEVHHQKLVFFAEDVGSNKGAIIGLMVGGVV) was also synthesized using Fmoc chemistry. Aβ42 peptide was purchased from Your Bio-Tech Partner, Shanghai, China, and used directly. All peptides were purified by reverse-phase HPLC (C_{18} column, Waters 600) and identified by matrix-assisted laser desorption ionization time-of-flight mass spectrometry (MALDI-TOF/TOF MS, ABI Research). All fibril samples (including the F_β and $F_{p\beta}$ fibrils) were prepared following the method described previously (80). Briefly, the Aβ or pAβ peptides were dissolved in HFIP (1 mg/ml, Sigma) for at least 4 h at ambient temperature to remove any preformed aggregates. Then the HFIP was removed by blow drying with N_2 and further vacuum drying for at least 3 h using an oil pump. The thin film of peptides was then resuspended in 20 mM Tris·HCl buffer, 150 mM NaCl, pH 7.4, and incubated at 37 °C with 200-rpm continuous shaking for 2 days to produce mature fibrils.

ThT Fluorescence Kinetics Assay—The ThT fluorescence kinetics assay was conducted on the Synergy 4 (BioTek) plate reader using a 96-well plate (λ_{ex} = 440 nm and λ_{em} = 480 nm). For monitoring the fibrillation process of Aβ and pAβ (40 μM), ThT signals (20 μM) were recorded at 37 °C under continuous shaking (medium) with a time interval of ~10 min between each recording. For tracking the aggregation process of different Aβ species (40 μM Aβ40, 10 μM Aβ(3pE)40, and 10 μM Aβ42) in the presence of F_β and $F_{p\beta}$ seeds (10%), the seeds of F_β and $F_{p\beta}$ were prepared by sonicating the resulted fibrils three times (1.5 min each time) in an ice bath. ThT signals were recorded at 37 °C under quiescent conditions with a time interval of 10 min between each recording. The fibrillation ThT kinetics curves of Aβ and pAβ were fitted using a sigmoidal function, $F - F_0 = 1/(1 + \exp(\gamma_{max}(\tau_{1/2} - t)))$, in which $\tau_{1/2}$ is the half-completion time of aggregation and γ_{max} is the maximum growth rate (50). The t_{lag} (lag time) was determined as the time intercept of the line best fitted to the linear portion of the F to t coordinate. All the experiments were replicated at least three times.

TEM—Fibrils samples (8 μl) were directly incubated on a carbon-coated copper grid for 2 min and then stained with 2% sodium phosphotungstic acid, pH 6.5, for 1 min. TEM images were recorded using a Hitachi-7650B electron microscope at 80 kV.

CD—CD spectroscopy in the 200–260-nm region (far-UV region) was performed with a Chirascan Plus CD spectrophotometer (Applied Photophysics). All samples (40 μM; 200 μl) were directly loaded in a 1-mm width CD cuvette, and signals were recorded at room temperature with three-scan signal averaging.

XRD—F_β and $F_{p\beta}$ fibrils were centrifuged (12,000 rpm) at 4 °C for 30 min, and the resulting pellets were washed with ddH_2O three times to remove salts. The pellets were then resuspended in 10 μl of ddH_2O, and the final suspension was aligned between two fire-polished glass rods at 4 °C overnight. XRD images were recorded on a Rigaku Micromax-007 X-ray generator equipped with an R-Axis IV++ area detector.

FT-IR Spectroscopy —FT-IR spectroscopy was performed on a Frontier FT-IR (PerkinElmer Life Sciences) equipped with an attenuated total reflectance accessory at ambient temperature. 1 ml of F_β and $F_{p\beta}$ fibrils was centrifuged (12,000 rpm) at 4 °C for 30 min. The pellets were then washed with ddH_2O three times to remove salts. The pellets were then frozen and dried into powders. The monomeric samples were prepared by dissolving Aβ and pAβ (1 mg/ml) in HFIP overnight, and then the solutions were frozen and lyophilized into powders. The final powders were directly loaded on the attenuated total reflectance accessory for acquisition of data.

Dephosphorylation by CIP—All samples with or without CIP (Sigma) were incubated at 37 °C for 30 min. The final mixtures were then directly loaded and analyzed using Tricine-SDS-PAGE and native PAGE, respectively. The PAGE images were recorded using VersaDoc 3000 (Bio-Rad). For all the experiments, 20 μl of 40 μM Aβ monomers or fibrils was used.

Neuronal Cell Toxicity Assay—To detect the toxicities of the two fibrils, the fibrils were centrifuged at 12,000 rpm at 4 °C for 1 h, and the final pellets were resuspended in the cell culture medium, sonicated in an ice bath three times (1.5 min each time). MTT reduction assays were used to determine the effects of F_β and $F_{p\beta}$ fibrils on viability of neuronal cells. Mouse neuroblastoma N2a cells and murine microglia BV-2 cells were plated at a density of 5000 cells/well on 96-well plates in 150 μl of culture medium (50% α-minimum Eagle's medium and 50% DMEM with 10% fetal bovine serum for N2a cells and 100% DMEM with 10% fetal bovine serum for BV-2 Cells). After 24-h incubation at 37 °C, the medium was exchanged for fresh medium (100% DMEM without fetal bovine serum) with F_β and $F_{p\beta}$ fibrils. After 24-h incubation, 20 μl of MTT (5 mg/ml) was added into each well for a further 4-h incubation. The culture medium was then discarded, and 150 μl of DMSO was added to

dissolving formazan completely. Absorbance at 490 nm was measured using Synergy 4 plate reader to calculate the cell viability.

MAS NMR—The seeded fibrils for MAS NMR measurements were prepared by incubating the isotope-labeled monomeric Aβ40 with 10% F_β and $F_{p\beta}$ seeds for 2 days quiescently. The fibrils were then centrifuged at 100,000 $\times$ *g* for 1 h at 4 °C (Beckman Coulter). The final pellets were freeze-dried and packed into 2.5-mm MAS rotors with rehydration using deionized water (1 μl/mg). All MAS NMR measurements were performed on a 600-MHz Bruker solid-state NMR spectrometer equipped with a 2.5-mm TriGamma MAS probe. The MAS frequency was set to 10 kHz for all experiments. The sample temperature was kept at $\sim$ 5 °C using a 270 K N_2 cooling line. The ^{31}P spectra were recorded using direct excitation with a 50-kHz ^{31}P 90° radiofrequency (rf) pulse and a 100-kHz continuous wave ^{1}H decoupling during the acquisition time. The two-dimensional (2D) ^{13}C-^{13}C spin diffusion spectra were recorded using a pulse sequence composed of a 60-kHz ^{1}H excitation 90° pulse, a linearly ramped ^{1}H-^{13}C cross-polarization period, a 10-kHz rf-assisted diffusion ^{1}H field during the 10-ms mixing period, and a 100-kHz ^{1}H two-pulse phase modulation decoupling. The ^{31}P and 2D spectra were processed using Topspin and NMRPipe software, respectively.

Author Contributions—Z.-W. H. synthesized the peptides, designed and conducted all experiments, and wrote the paper. M.-R. M. contributed to the XRD and CD experiments. Y.-X. C. and Y.-F. Z. analyzed the results and revised the paper intellectually. W. Q. designed and conducted the NMR experiments, analyzed the results, and wrote the paper. Y.-M. L. conceived the project, designed all the experiments, and wrote the paper. All authors reviewed the results and approved the final version of the manuscript.

Acknowledgment—We sincerely acknowledge Dr. Cong Liu (Interdisciplinary Research Center on Biology and Chemistry, Shanghai Institute of Organic Chemistry, Chinese Academy of Sciences, China) for kind help with XRD measurement and very useful discussions.

References

1. Chiti, F., and Dobson, C. M. (2006) Protein misfolding, functional amyloid, and human disease. *Annu. Rev. Biochem.* **75,** 333–366
2. Eisenberg, D., and Jucker, M. (2012) The amyloid state of proteins in human diseases. *Cell* **148,** 1188–1203
3. Guo, J. L., and Lee, V. M. (2014) Cell-to-cell transmission of pathogenic proteins in neurodegenerative diseases. *Nat. Med.* **20,** 130–138
4. Knowles, T. P., Vendruscolo, M., and Dobson, C. M. (2014) The amyloid state and its association with protein misfolding diseases. *Nat. Rev. Mol. Cell Biol.* **15,** 384–396
5. Kodali, R., and Wetzel, R. (2007) Polymorphism in the intermediates and products of amyloid assembly. *Curr. Opin. Struct. Biol.* **17,** 48–57
6. Tycko, R. (2015) Amyloid polymorphism: structural basis and neurobiological relevance. *Neuron* **86,** 632–645
7. Nekooki-Machida, Y., Kurosawa, M., Nukina, N., Ito, K., Oda, T., and Tanaka, M. (2009) Distinct conformations of *in vitro* and *in vivo* amyloids of huntingtin-exon1 show different cytotoxicity. *Proc. Natl. Acad. Sci. U.S.A.* **106,** 9679–9684
8. Petkova, A. T., Leapman, R. D., Guo, Z., Yau, W. M., Mattson, M. P., and Tycko, R. (2005) Self-propagating, molecular-level polymorphism in Alzheimer's β-amyloid fibrils. *Science* **307,** 262–265
9. Bousset, L., Pieri, L., Ruiz-Arlandis, G., Gath, J., Jensen, P. H., Habenstein, B., Madiona, K., Olieric, V., Böckmann, A., Meier, B. H., and Melki, R. (2013) Structural and functional characterization of two α-synuclein strains. *Nat. Commun.* **4,** 2575
10. Stöhr, J., Condello, C., Watts, J. C., Bloch, L., Oehler, A., Nick, M., DeArmond, S. J., Giles, K., DeGrado, W. F., and Prusiner, S. B. (2014) Distinct synthetic Aβ prion strains producing different amyloid deposits in bigenic mice. *Proc. Natl. Acad. Sci. U.S.A.* **111,** 10329–10334
11. Guo, J. L., Covell, D. J., Daniels, J. P., Iba, M., Stieber, A., Zhang, B., Riddle, D. M., Kwong, L. K., Xu, Y., Trojanowski, J. Q., and Lee, V. M. (2013) Distinct α-synuclein strains differentially promote tau inclusions in neurons. *Cell* **154,** 103–117
12. Frost, B., and Diamond, M. I. (2010) Prion-like mechanisms in neurodegenerative diseases. *Nat. Rev. Neurosci.* **11,** 155–159
13. Goedert, M., Clavaguera, F., and Tolnay, M. (2010) The propagation of prion-like protein inclusions in neurodegenerative diseases. *Trends Neurosci.* **33,** 317–325
14. Polymenidou, M., and Cleveland, D. W. (2012) Prion-like spread of protein aggregates in neurodegeneration. *J. Exp. Med.* **209,** 889–893
15. Chien, P., Weissman, J. S., and DePace, A. H. (2004) Emerging principles of conformation-based prion inheritance. *Annu. Rev. Biochem.* **73,** 617–656
16. Brettschneider, J., Del Tredici, K., Lee, V. M., and Trojanowski, J. Q. (2015) Spreading of pathology in neurodegenerative diseases: a focus on human studies. *Nat. Rev. Neurosci.* **16,** 109–120
17. Sanders, D. W., Kaufman, S. K., Holmes, B. B., and Diamond, M. I. (2016) Prions and protein assemblies that convey biological information in health and disease. *Neuron* **89,** 433–448
18. Xue, W.-F., Hellewell, A. L., Gosal, W. S., Homans, S. W., Hewitt, E. W., and Radford, S. E. (2009) Fibril fragmentation enhances amyloid cytotoxicity. *J. Biol. Chem.* **284,** 34272–34282
19. Kalapothakis, J. M., Morris, R. J., Szavits-Nossan, J., Eden, K., Covill, S., Tabor, S., Gillam, J., Barran, P. E., Allen, R. J., and MacPhee, C. E. (2015) A kinetic study of ovalbumin fibril formation: the importance of fragmentation and end-joining. *Biophys. J.* **108,** 2300–2311
20. Cras, P., Kawai, M., Lowery, D., Gonzalez-DeWhitt, P., Greenberg, B., and Perry, G. (1991) Senile plaque neurites in Alzheimer disease accumulate amyloid precursor protein. *Proc. Natl. Acad. Sci. U.S.A.* **88,** 7552–7556
21. Yin, R. H., Tan, L., Jiang, T., and Yu, J. T. (2014) Prion-like mechanisms in Alzheimer's disease. *Curr. Alzheimer Res.* **11,** 755–764
22. Jaunmuktane, Z., Mead, S., Ellis, M., Wadsworth, J. D., Nicoll, A. J., Kenny, J., Launchbury, F., Linehan, J., Richard-Loendt, A., Walker, A. S., Rudge, P., Collinge, J., and Brandner, S. (2015) Evidence for human transmission of amyloid-β pathology and cerebral amyloid angiopathy. *Nature* **525,** 247–250
23. Paravastu, A. K., Qahwash, I., Leapman, R. D., Meredith, S. C., and Tycko, R. (2009) Seeded growth of β-amyloid fibrils from Alzheimer's brain-derived fibrils produces a distinct fibril structure. *Proc. Natl. Acad. Sci. U.S.A.* **106,** 7443–7448
24. Lu, J. X., Qiang, W., Yau, W. M., Schwieters, C. D., Meredith, S. C., and Tycko, R. (2013) Molecular structure of β-amyloid fibrils in Alzheimer's disease brain tissue. *Cell* **154,** 1257–1268
25. Watts, J. C., Condello, C., Stöhr, J., Oehler, A., Lee, J., DeArmond, S. J., Lannfelt, L., Ingelsson, M., Giles, K., and Prusiner, S. B. (2014) Serial propagation of distinct strains of Aβ prions from Alzheimer's disease patients. *Proc. Natl. Acad. Sci. U.S.A.* **111,** 10323–10328
26. Cohen, M., Appleby, B., and Safar, J. G. (2016) Distinct prion-like strains of amyloid β implicated in phenotypic diversity of Alzheimer's disease. *Prion* **10,** 9–17
27. Xiao, Y., Ma, B., McElheny, D., Parthasarathy, S., Long, F., Hoshi, M., Nussinov, R., and Ishii, Y. (2015) Aβ(1–42) fibril structure illuminates self-recognition and replication of amyloid in Alzheimer's disease. *Nat. Struct. Mol. Biol.* **22,** 499–505
28. Meyer-Luehmann, M., Coomaraswamy, J., Bolmont, T., Kaeser, S., Schaefer, C., Kilger, E., Neuenschwander, A., Abramowski, D., Frey, P., Jaton, A. L., Vigouret, J. M., Paganetti, P., Walsh, D. M., Mathews, P. M., Ghiso, J., *et al.* (2006) Exogenous induction of cerebral β-amyloidogenesis is governed by agent and host. *Science* **313,** 1781–1784

29. Eisele, Y. S., Obermüller, U., Heilbronner, G., Baumann, F., Kaeser, S. A., Wolburg, H., Walker, L. C., Staufenbiel, M., Heikenwalder, M., and Jucker, M. (2010) Peripherally applied Aβ-containing inoculates induce cerebral β-amyloidosis. *Science* **330,** 980–982
30. Stöhr, J., Watts, J. C., Mensinger, Z. L., Oehler, A., Grillo, S. K., DeArmond, S. J., Prusiner, S. B., and Giles, K. (2012) Purified and synthetic Alzheimer's amyloid β (Aβ) prions. *Proc. Natl. Acad. Sci. U.S.A.* **109,** 11025–11030
31. Kumar, S., and Walter, J. (2011) Phosphorylation of amyloid β (Aβ) peptides—a trigger for formation of toxic aggregates in Alzheimer's disease. *Aging* **3,** 803–812
32. Jawhar, S., Wirths, O., and Bayer, T. A. (2011) Pyroglutamate amyloid-β (Aβ): a hatchet man in Alzheimer disease. *J. Biol. Chem.* **286,** 38825–38832
33. Bah, A., Vernon, R. M., Siddiqui, Z., Krzeminski, M., Muhandiram, R., Zhao, C., Sonenberg, N., Kay, L. E., and Forman-Kay, J. D. (2015) Folding of an intrinsically disordered protein by phosphorylation as a regulatory switch. *Nature* **519,** 106–109
34. Kardos, J., Kiss, B., Micsonai, A., Rovó, P., Menyhárd, D. K., Kovács, J., Váradi, G., Tóth, G. K., and Perczel, A. (2015) Phosphorylation as conformational switch from the native to amyloid state: Trp-cage as a protein aggregation model. *J. Phys. Chem. B* **119,** 2946–2955
35. Du, J. T., Li, Y. M., Wei, W., Wu, G. S., Zhao, Y. F., Kanazawa, K., Nemoto, T., and Nakanishi, H. (2005) Low-barrier hydrogen bond between phosphate and the amide group in phosphopeptide. *J. Am. Chem. Soc.* **127,** 16350–16351
36. Gandhi, N. S., Landrieu, I., Byrne, C., Kukic, P., Amniai, L., Cantrelle, F.-X., Wieruszeski, J.-M., Mancera, R. L., Jacquot, Y., and Lippens, G. (2015) A phosphorylation-induced turn defines the Alzheimer's disease AT8 antibody epitope on the tau protein. *Angew. Chem. Int. Ed. Engl.* **54,** 6819–6823
37. Rezaei-Ghaleh, N., Amininasab, M., Giller, K., Kumar, S., Stündl, A., Schneider, A., Becker, S., Walter, J., and Zweckstetter, M. (2014) Turn plasticity distinguishes different modes of amyloid-β aggregation. *J. Am. Chem. Soc.* **136,** 4913–4919
38. Zhou, L.-X., Zeng, Z.-Y., Du, J.-T., Zhao, Y.-F., and Li, Y.-M. (2006) The self-assembly ability of the first microtubule-binding repeat from tau and its modulation by phosphorylation. *Biochem. Biophys. Res. Commun.* **348,** 637–642
39. Du, J.-T., Yu, C.-H., Zhou, L.-X., Wu, W.-H., Lei, P., Li, Y., Zhao, Y.-F., Nakanishi, H., and Li, Y.-M. (2007) Phosphorylation modulates the local conformation and self-aggregation ability of a peptide from the fourth tau microtubule-binding repeat. *FEBS J.* **274,** 5012–5020
40. Ma, M.-R., Hu, Z.-W., Zhao, Y.-F., Chen, Y.-X., and Li, Y.-M. (2016) Phosphorylation induces distinct α-synuclein strain formation. *Sci. Rep.* **6,** 37130
41. Milton, N. G. (2005) Phosphorylated amyloid-β: the toxic intermediate in Alzheimer's disease neurodegeneration. *Subcell. Biochem.* **38,** 381–402
42. Kumar, S., Wirths, O., Theil, S., Gerth, J., Bayer, T. A., and Walter, J. (2013) Early intraneuronal accumulation and increased aggregation of phosphorylated Aβ in a mouse model of Alzheimer's disease. *Acta Neuropathol.* **125,** 699–709
43. Rijal Upadhaya, A., Kosterin, I., Kumar, S., von Arnim, C. A., Yamaguchi, H., Fändrich, M., Walter, J., and Thal, D. R. (2014) Biochemical stages of amyloid-β peptide aggregation and accumulation in the human brain and their association with symptomatic and pathologically preclinical Alzheimer's disease. *Brain* **137,** 887–903
44. Kumar, S., Rezaei-Ghaleh, N., Terwel, D., Thal, D. R., Richard, M., Hoch, M., McDonald, J. M., Wüllner, U., Glebov, K., Heneka, M. T., Walsh, D. M., Zweckstetter, M., and Walter, J. (2011) Extracellular phosphorylation of the amyloid β-peptide promotes formation of toxic aggregates during the pathogenesis of Alzheimer's disease. *EMBO J.* **30,** 2255–2265
45. Kumar, S., Singh, S., Hinze, D., Josten, M., Sahl, H. G., Siepmann, M., and Walter, J. (2012) Phosphorylation of amyloid-β peptide at serine 8 attenuates its clearance via insulin-degrading and angiotensin-converting enzymes. *J. Biol. Chem.* **287,** 8641–8651
46. Rezaei-Ghaleh, N., Amininasab, M., Kumar, S., Walter, J., and Zweckstetter, M. (2016) Phosphorylation modifies the molecular stability of β-amyloid deposits. *Nat. Commun.* **7,** 11359
47. Sanders, D. W., Kaufman, S. K., DeVos, S. L., Sharma, A. M., Mirbaha, H., Li, A., Barker, S. J., Foley, A. C., Thorpe, J. R., Serpell, L. C., Miller, T. M., Grinberg, L. T., Seeley, W. W., and Diamond, M. I. (2014) Distinct tau prion strains propagate in cells and mice and define different tauopathies. *Neuron* **82,** 1271–1288
48. Peelaerts, W., Bousset, L., Van der Perren, A., Moskalyuk, A., Pulizzi, R., Giugliano, M., Van den Haute, C., Melki, R., and Baekelandt, V. (2015) α-Synuclein strains cause distinct synucleinopathies after local and systemic administration. *Nature* **522,** 340–344
49. Serpell, L. C., Berriman, J., Jakes, R., Goedert, M., and Crowther, R. A. (2000) Fiber diffraction of synthetic α-synuclein filaments shows amyloid-like cross-β conformation. *Proc. Natl. Acad. Sci. U.S.A.* **97,** 4897–4902
50. Abelein, A., Jarvet, J., Barth, A., Gräslund, A., and Danielsson, J. (2016) Ionic strength modulation of the free energy landscape of Aβ40 peptide fibril formation. *J. Am. Chem. Soc.* **138,** 6893–6902
51. Sarroukh, R., Goormaghtigh, E., Ruysschaert, J.-M., and Raussens, V. (2013) ATR-FTIR: a "rejuvenated" tool to investigate amyloid proteins. *Biochim. Biophys. Acta* **1828,** 2328–2338
52. Matsuzaki, K. (2014) How do membranes initiate Alzheimer's disease? Formation of toxic amyloid fibrils by the amyloid β-protein on ganglioside clusters. *Acc. Chem. Res.* **47,** 2397–2404
53. Xu, F., Fu, Z., Dass, S., Kotarba, A. E., Davis, J., Smith, S. O., and Van Nostrand, W. E. (2016) Cerebral vascular amyloid seeds drive amyloid β-protein fibril assembly with a distinct anti-parallel structure. *Nat. Commun.* **7,** 13527
54. Makin, O. S., Atkins, E., Sikorski, P., Johansson, J., and Serpell, L. C. (2005) Molecular basis for amyloid fibril formation and stability. *Proc. Natl. Acad. Sci. U.S.A.* **102,** 315–320
55. Rezaei-Ghaleh, N., Kumar, S., Walter, J., and Zweckstetter, M. (2016) Phosphorylation interferes with maturation of amyloid-β fibrillar structure in the N-terminus. *J. Biol. Chem.* **291,** 16059–16067
56. Zalatan, J. G., and Herschlag, D. (2006) Alkaline phosphatase mono- and diesterase reactions: comparative transition state analysis. *J. Am. Chem. Soc.* **128,** 1293–1303
57. Chaudhuri, G., Chatterjee, S., Venu-Babu, P., Ramasamy, K., and Thilagaraj, W. R. (2013) Kinetic behaviour of calf intestinal alkaline phosphatase with pNPP. *Indian J. Biochem. Biophys.* **50,** 64–71
58. Olzscha, H., Schermann, S. M., Woerner, A. C., Pinkert, S., Hecht, M. H., Tartaglia, G. G., Vendruscolo, M., Hayer-Hartl, M., Hartl, F. U., and Vabulas, R. M. (2011) Amyloid-like aggregates sequester numerous metastable proteins with essential cellular functions. *Cell* **144,** 67–78
59. Rahman, M. M., Zetterberg, H., Lendel, C., and Härd, T. (2015) Binding of human proteins to amyloid-β protofibrils. *ACS Chem. Biol.* **10,** 766–774
60. Zorn, J. A., Wille, H., Wolan, D. W., and Wells, J. A. (2011) Self-assembling small molecules form nanofibrils that bind procaspase-3 to promote activation. *J. Am. Chem. Soc.* **133,** 19630–19633
61. Julien, O., Kampmann, M., Bassik, M. C., Zorn, J. A., Venditto, V. J., Shimbo, K., Agard, N. J., Shimada, K., Rheingold, A. L., Stockwell, B. R., Weissman, J. S., and Wells, J. A. (2014) Unraveling the mechanism of cell death induced by chemical fibrils. *Nat. Chem. Biol.* **10,** 969–976
62. Colby, D. W., Zhang, Q., Wang, S., Groth, D., Legname, G., Riesner, D., and Prusiner, S. B. (2007) Prion detection by an amyloid seeding assay. *Proc. Natl. Acad. Sci. U.S.A.* **104,** 20914–20919
63. Nussbaum, J. M., Schilling, S., Cynis, H., Silva, A., Swanson, E., Wangsanut, T., Tayler, K., Wiltgen, B., Hatami, A., Rönicke, R., Reymann, K., Hutter-Paier, B., Alexandru, A., Jagla, W., Graubner, S., *et al.* (2012) Prion-like behaviour and tau-dependent cytotoxicity of pyroglutamylated amyloid-β. *Nature* **485,** 651–655
64. Qiang, W., Yau, W. M., and Tycko, R. (2011) Structural evolution of Iowa mutant β-amyloid fibrils from polymorphic to homogeneous states under repeated seeded growth. *J. Am. Chem. Soc.* **133,** 4018–4029
65. Cohen, S. I., Linse, S., Luheshi, L. M., Hellstrand, E., White, D. A., Rajah, L., Otzen, D. E., Vendruscolo, M., Dobson, C. M., and Knowles, T. P. (2013) Proliferation of amyloid-β42 aggregates occurs through a secondary nucleation mechanism. *Proc. Natl. Acad. Sci. U.S.A.* **110,** 9758–9763
66. Esler, W. P., Stimson, E. R., Jennings, J. M., Vinters, H. V., Ghilardi, J. R., Lee, J. P., Mantyh, P. W., and Maggio, J. E. (2000) Alzheimer's disease amyloid propagation by a template-dependent dock-lock mechanism. *Biochemistry* **39,** 6288–6295

67. Nguyen, P. H., Li, M. S., Stock, G., Straub, J. E., and Thirumalai, D. (2007) Monomer adds to preformed structured oligomers of Aβ-peptides by a two-stage dock-lock mechanism. *Proc. Natl. Acad. Sci. U.S.A.* **104,** 111–116
68. O'Brien, E. P., Okamoto, Y., Straub, J. E., Brooks, B. R., and Thirumalai, D. (2009) Thermodynamic perspective on the dock-lock growth mechanism of amyloid fibrils. *J. Phys. Chem. B* **113,** 14421–14430
69. Paravastu, A. K., Leapman, R. D., Yau, W. M., and Tycko, R. (2008) Molecular structural basis for polymorphism in Alzheimer's β-amyloid fibrils. *Proc. Natl. Acad. Sci. U.S.A.* **105,** 18349–18354
70. Qiang, W., Kelley, K., and Tycko, R. (2013) Polymorph-specific kinetics and thermodynamics of β-amyloid fibril growth. *J. Am. Chem. Soc.* **135,** 6860–6871
71. Zhang, S., Andreasen, M., Nielsen, J. T., Liu, L., Nielsen, E. H., Song, J., Ji, G., Sun, F., Skrydstrup, T., Besenbacher, F., Nielsen, N. C., Otzen, D. E., and Dong, M. (2013) Coexistence of ribbon and helical fibrils originating from hIAPP(20–29) revealed by quantitative nanomechanical atomic force microscopy. *Proc. Natl. Acad. Sci. U.S.A.* **110,** 2798–2803
72. Spirig, T., Ovchinnikova, O., Vagt, T., and Glockshuber, R. (2014) Direct evidence for self-propagation different amyloid-β fibril conformations. *Neurodegener. Dis.* **14,** 151–159
73. Petkova, A. T., Yau, W. M., and Tycko, R. (2006) Experimental constraints on quaternary structure in Alzheimer's β-amyloid fibrils. *Biochemistry* **45,** 498–512
74. Qiang, W., Yau, W. M., Luo, Y., Mattson, M. P., and Tycko, R. (2012) Antiparallel β-sheet architecture in Iowa-mutant β-amyloid fibrils. *Proc. Natl. Acad. Sci. U.S.A.* **109,** 4443–4448
75. Sgourakis, N. G., Yau, W. M., and Qiang, W. (2015) Modeling an in-register, parallel "Iowa" Aβ fibril structure using solid-state NMR data from labeled samples with Rosetta. *Structure* **23,** 216–227
76. Akinlolu, R. D., Nam, M., and Qiang, W. (2015) Competition between fibrillation and induction of vesicle fusion for the membrane-associated 40-residue β-amyloid peptides. *Biochemistry* **54,** 3416–3419
77. Shim, S. H., Gupta, R., Ling, Y. L., Strasfeld, D. B., Raleigh, D. P., and Zanni, M. T. (2009) Two-dimensional IR spectroscopy and isotope labeling defines the pathway of amyloid formation with residue-specific resolution. *Proc. Natl. Acad. Sci. U.S.A.* **106,** 6614–6619
78. Tanaka, M., and Komi, Y. (2015) Layers of structure and function in protein aggregation. *Nat. Chem. Biol.* **11,** 373–377
79. Kummer, M. P., Hermes, M., Delekarte, A., Hammerschmidt, T., Kumar, S., Terwel, D., Walter, J., Pape, H. C., König, S., Roeber, S., Jessen, F., Klockgether, T., Korte, M., and Heneka, M. T. (2011) Nitration of tyrosine 10 critically enhances amyloid β aggregation and plaque formation. *Neuron* **71,** 833–844
80. Jan, A., Hartley, D. M., and Lashuel, H. A. (2010) Preparation and characterization of toxic Aβ aggregates for structural and functional studies in Alzheimer's disease research. *Nat. Protoc.* **5,** 1186–1209